Available online at www.sciencedirect.com
ScienceDirect
Sensors and Actuators B 121 (2007) 330–340
SENSORS AND ACTUATORS B CHEMICAL
www.elsevier.com/locate/snb

# Physiochemical microparticle sensors based on nonlinear magnetic oscillations

Brandon H. McNaughton [a,b], Rodney R. Agayan [a,b], Jane X. Wang [a,b], Raoul Kopelman [a,b,*]

[a] The University of Michigan, Applied Physics Program, 2477 Randall Laboratory, Ann Arbor, MI 48109-1120, United States
[b] The University of Michigan, Department of Chemistry, 930 North University, Ann Arbor, MI 48109-1055, United States

Available online 20 October 2006

**Abstract**

Recently, the nonlinear rotation of single magnetic particles has emerged as a tool to measure physical parameters on the micro-scale. In this paper, detailed theoretical analyses are carried out for tailored microprobes that measure (1) local magnetic fields, (2) magnetic particle characteristics, (3) viscosity and (4) chemical binding, along with their corresponding experimental demonstrations. Such new physical measurement methods, using single micro- or nano-particles, in combination with previous chemical nanoparticle sensing methods, lead to a new class of physiochemical micro- and nano-particle sensors that may be of significant biomedical and technological interest.


*Keywords:* Critical phase-slipping; Nonlinear rotation; Physiochemical sensor; Non-uniform oscillator; Magnetic nanoparticles; Magnetic microspheres

## 1. Introduction

Magnetic microspheres and nanoparticles have numerous practical uses, ranging from medical [1–4] to magnetic recording [5] applications. While there is a variety of existing and developing applications, most utilize ensemble properties of the particles. Alternatively, monitoring the rotational behavior of single magnetic particles or a chain of several particles, through standard microscopy techniques, for example, has lead to a new range of potential applications [8]. One behavior of magnetic particles that has been theoretically treated [7,8] but not fully utilized is the nonlinear rotation of a magnetic particle aligning with an external rotating magnetic field in a viscous fluid. For lower external rotation rates, the phase of the rotation of the particle remains locked to that of the external field. Nonlinear rotation occurs at sufficiently high external rotation rates when the magnetic particle cannot overcome the viscous drag, i.e. it cannot keep up with the external field's rotation rate. The phase between the external field and the particle's moment "slips," and the rotation becomes asynchronous with the external field. The transition from synchronous to asynchronous rotation occurs at an abrupt "critical slipping rate" which depends on physical properties like the viscosity of the environment and the volume, shape, and magnetic moment of the particle.

In previous work we attempted to combine the critical phase-slipping behavior of single magnetic particles with chemical sensing in order to create a physiochemical sensor [8]. This type of sensor could be used to elucidate new physical and chemical interactions in biological environments still not fully understood [9]. For instance, solid state chemical sensors can be coated with a thin layer of magnetic material adding an extra dimension of physical sensing [10]. While there has been much work on chemical microsensors [11–15], relatively few applications of nonlinear micro-oscillators have been demonstrated. Here, we hope to lay the foundation for using nonlinear micro-oscillators as physical sensors so that the two types of sensors, physical and chemical, can be combined.

Often monitored with optical microscopy, micro-oscillators are typically rotated in one of two planes: parallel or perpendicular to the imaging plane. To determine whether the particles are phase-locking (linear rotation) or phase-slipping (nonlinear rotation), one can rotate an asymmetrical particle in the plane of the sample [8,16–18]—see top of Fig. 1. Image analysis software can then be used to track the orientation in time allowing calculation of the average rotation rate. An alternative technique for linear and nonlinear rotation of magnetic microparticles is to rotate spherically symmetric, but optically asymmetric

* Corresponding author at: The University of Michigan, Department of Chemistry, 930 North University, Ann Arbor, MI 48109-1055, United States.
Tel.: +1 734 764 7541; fax: +1 734 936 2778.
*E-mail address:* kopelman@umich.edu (R. Kopelman).

0925-4005/$ – see front matter © 2006 Elsevier B.V. All rights reserved.
doi:10.1016/j.snb.2006.09.043

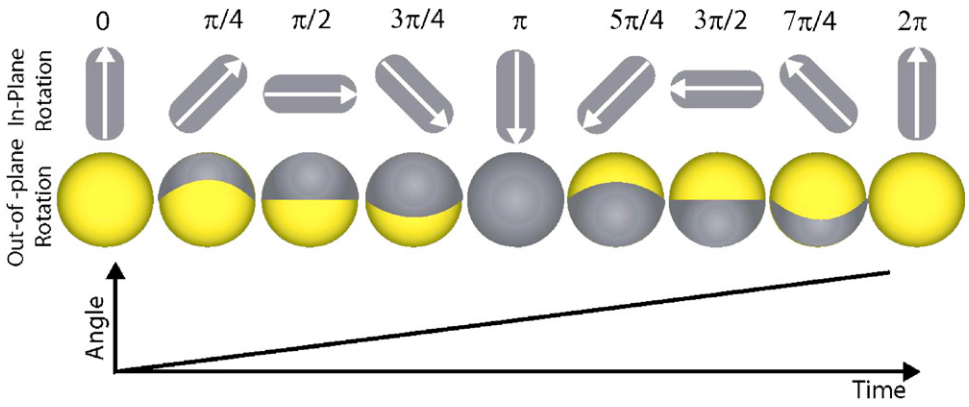


Fig. 1. Schematic of phase-locked rotation, below the critical slipping rate, for two types of particles. Each type is rotated in a different plane: (top row) an asymmetric particle rotating in the image plane and (middle row) a physically symmetric, but optically asymmetric particle rotating in a plane orthogonal to the image plane. In both cases the orientation and average rotation rate will be identical (bottom), allowing either technique to be used for phase-locking and phase-slipping experiments.

spheres in a plane that is perpendicular to the imaging plane [6]—see bottom of Fig. 1. The tailor made probes are particles that emit or reflect varying intensities of light, depending on their angular orientation [10,19]. This probe anisotropy can be accomplished in a variety of ways, but generally these types of probes have been referred to as MagMOONs [6,10,19–26], crescent moons [27], capped colloids [28], Janus particles [29–31], and half-shells [32,33]. By tracking the intensity of an optically anisotropic magnetic particle as it rotates, the orientation and average rotation rate can be determined; thus, phase-locking and phase-slipping can be monitored for quasi-spherical particles [6]. In this paper we mainly utilize out-of-plane rotation. All applications and theory discussed in this paper can be performed with any optically or physically anisotropic magnetic particle rotated in either plane.

Several groups have already studied the linear-to-nonlinear rotation of various systems. Shelton and colleagues used polarized light to torque a glass nanorod. They formed a theory of motion for the rotating nanorod and found both theoretically and experimentally that the average rotation rate of the glass rod had a nonlinear dependence on the rotation rate of the polarized light [18]. Biswal and Gast used a chain of paramagnetic particles to mix fluids and showed that properties of mixing were affected by the nonlinear oscillations of the chain [16]. Korneva et al. have used the critical slipping rate to estimate the magnetization of carbon nanotubes filled with magnetic nanoparticles [17]. In our lab we have observed linear and nonlinear rotation using ~4.4 μm spherical fluorescent magnetic particles [6]. While the above experiments have described, in various ways, the linear-to-nonlinear rotation of single particles and single systems of particles, a thorough investigation into the phenomenon of single magnetic particle rotations and their respective applications has yet to be carried out. This is especially true concerning the use of asynchronous rotation to perform real-time physical measurements (see Section 2.5). Therefore, we present here a theoretical model that describes the rotational dynamics of single magnetic particles, with the specific aim of elucidating and demonstrating the inherent applications.

## 2. Theoretical review

### 2.1. Equation of motion

While there are well-developed theories on rotating magnetic systems [7,8,34–36,54], few application-oriented theories or experiments for single particle systems that exhibit nonlinear rotations have been published. Cēbers and Ozols have performed a rigorous theoretical analysis on single particle systems, but did not focus on applications except to describe rotation of magnetobacteria and to suggest mass transfer applications [7]. In this section, the theory for a single magnetic particle is reviewed and several promising applications are discussed.

We begin with the magnetic torque that acts on a magnetic probe, which is given by

$$|\Gamma_{\mathrm{mag}}| = |\boldsymbol{m} \times \boldsymbol{B}| = mB\sin(\Omega t - \theta), \tag{1}$$

where $m$ is the magnetic moment, $B$ the external magnetic field, and $\Omega t - \theta$ is the angle between the external field and the magnetic moment, as defined in Fig. 2. If the external magnetic field is much smaller than that required to remagnetize the magnetic probe while the torque is larger than the Brownian torques, then

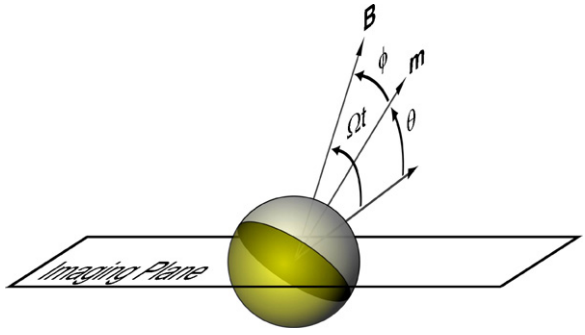


Fig. 2. Schematic representation of a rotationally driven magnetic particle, where the phase lag is given by $\Omega t - \theta$. The external field is represented by $\boldsymbol{B}$ and the magnetization of the magnetic microsphere is $\boldsymbol{m}$.

the equation of motion is given by [35]

$$I\ddot{\theta} - \gamma\dot{\theta} + mB\sin(\Omega t - \theta) = 0, \tag{2}$$

where $I$ is the moment of inertia and $\gamma$ is the drag coefficient. To simplify the number of parameters, Eq. (2) can be made dimensionless by allowing

$$\Omega_c = \frac{mB}{\gamma}, \qquad \tau = \Omega_c t, \quad \text{and} \quad \phi = \Omega t - \theta. \tag{3}$$

Given these expressions, Eq. (2) can be expressed as

$$\frac{-I\Omega_c}{\gamma}\frac{d^2\phi}{d\tau^2} + \frac{d\phi}{d\tau} = \frac{\Omega}{\Omega_c} - \sin(\phi). \tag{4}$$

### 2.2. Reynolds number

For most magnetic micro- and nano-particles, the inertial term in Eq. (4) is negligible. This can be verified by calculating the Reynolds number, a dimensionless quantity equal to the ratio of the inertial force to the drag force; for a rotating sphere the Reynolds number is

$$Re = \frac{r^2\rho\dot{\theta}}{\eta} = \frac{r^2\dot{\theta}}{\nu}, \tag{5}$$

where $r$ is the radius of a sphere, $\rho$ the density of the fluid, $\dot{\theta}$ the rotation rate of the sphere, $\eta$ the dynamic viscosity, and $\nu$ is the kinematic viscosity. A low Reynolds number is equivalent to the condition $(I\Omega_c/\gamma) \ll 1$ from Eq. (4). For example, a typical 5.0 μm magnetic microsphere in pure glycerol at 20 °C, which has a reported kinematic viscosity of 1160 cSt [37], rotating at ~63 rad/s (10 rotations/s) will have a Reynolds number of $\sim 3.4 \times 10^{-7}$. Thus, the condition that allows inertia to be neglected, $Re \ll 1$, is satisfied. In all low Reynolds number environments, such inertial effects are negligible [38]. When smaller spheres are used, $Re$ becomes even less significant. The experiments performed in this paper had negligible inertia due to low Reynolds numbers.

### 2.3. Nonuniform oscillator equation

From Section 2.2, it is clear that the system under investigation is in a low Reynolds number regime and inertia can be ignored. Ignoring inertia allows Eq. (4) to be rewritten in the form of the nonuniform oscillator equation

$$\frac{d\phi}{d\tau} = \frac{\Omega}{\Omega_c} - \sin(\phi), \tag{6}$$

which also describes voltages across a Josephson Junction [39], the optical torquing of a glass nanorod [18], and even the flashing of a firefly [39]. One measurable quantity of optically anisotropic particles is the intensity modulation produced as they rotate. This intensity depends on the particle's orientation angle, which can be calculated, but it is more straightforward to measure the average rotation rate from the particle's intensity. Given Eq. (6), the period of rotation and, therefore, the average rotation rate can be determined. The period is given by

$$T = \int dt = \frac{1}{\Omega_c}\int \frac{d\tau}{d\phi}d\phi = \int_0^{2\pi} \frac{d\phi}{\Omega - \Omega_c\,\sin(\phi)} = \frac{2\pi}{\sqrt{\Omega^2 - \Omega_c^2}}. \tag{7}$$

Therefore, the average rotation rate, which is represented as $\langle d\theta/dt\rangle$, can be solved for rates both above and below the critical slipping rate. These two solutions are given by

$$\left\langle \frac{d\theta}{dt} \right\rangle = \begin{cases} \Omega & \Omega < \Omega_c \\ \Omega - \sqrt{\Omega^2 - \Omega_c^2} & \Omega > \Omega_c \end{cases}. \tag{8}$$

If inertia is kept in Eq. (4), then numerical integration methods such as the Runge–Kutta method can be used to determine $\langle d\theta/dt\rangle$. When inertia is considered, then $\Omega_c$ will depend on the direction from which the critical value is approached [39]. This arises from the inertia of the particle undergoing rotation, which would oppose the particle's tendency to realign with the external field. While this numerical solution has not been performed for spherical probes, it has been numerically solved and experimented with in order to determine the critical slipping of a magnetic microdrill (a cylindrical magnet with a spiral blade wrapped around its body, which is on the order of a millimeter in diameter) [40,41]. No experiments have been carried out, however, to show this hysteresis-like behavior. While critical phase-slipping has been studied at various size scales and Reynolds numbers, the authors are unaware of any study that experimentally shows the hysteresis of critical phase-slipping for microparticles.

The analysis performed in this section is valid for all the systems studied in this paper. The conditions and environments where the analysis is valid can be further clarified by defining a Reynolds number based on the maximum rotation rate of a rotating particle. This maximum rotation is given by $\Omega_c$; therefore, Eq. (5) can be rewritten as

$$Re_{max} = \frac{r^2\dot{\theta}_{max}}{\nu} = \frac{r^2\Omega_c}{\nu} = \frac{mBr^2}{\kappa V\rho\nu^2}, \tag{9}$$

where $\kappa$ is the shape factor, $\rho$ the density of the fluid, and $V$ is the volume of the particle. For a sphere, this becomes

$$Re_{max} = \frac{mB}{8\pi r\rho\nu^2}. \tag{10}$$

The value calculated from Eq. (10) is significant because it gives the highest value that the Reynolds number can have in a given system. Therefore, it is a good indicator of whether or not inertia can be ignored at all rotation rates.

### 2.4. Rotation of ellipsoidal shapes

The critical slipping rate can be determined for a variety of shapes, sizes and conditions. For example, an ellipsoid will have a different critical slipping rate than that of a similarly sized sphere due to the change in the shape factor. For a particle

rotating in a low Reynolds number environment, this point of criticality is given by

$$\Omega_c = \frac{mB}{\kappa\eta V}, \tag{11}$$

where for an ellipsoid with major axis $a$ and minor axis $b$, $\kappa$ can be determined from the equation [35]

$$\kappa = \frac{1.6\left[3(a/b)^2+2\right]}{1+\zeta-0.5\zeta(b/a)^2} \tag{12}$$

where

$$\zeta = \frac{1}{\varepsilon^3}\left[\ln\left(\frac{1+\varepsilon}{1-\varepsilon}\right)-2\varepsilon\right] \tag{13}$$

and

$$\varepsilon = \sqrt{1-(b/a)^2}, \quad (a \geq b). \tag{14}$$

For a sphere, $a=b$ and the shape factor becomes 6. Another example is a chain of $N$ spheres, and for $N \geq 3$ the shape factor is given by [16]

$$\kappa = \frac{2N^2}{\ln(N/2)} \tag{15}$$

This would result in a modified critical slipping rate of

$$\Omega_c = \frac{\ln(N/2)mB}{2N^2\eta V} \tag{16}$$

### 2.5. Real-time measurements by nonlinear rotation

The entire rotational behavior of single particles can be measured to determine the value of the critical slipping rate. This technique involves measuring the rotation response of a magnetic microsphere at varying external driving frequencies (see Section 3.4 and refs. [8] and [18]). It is also possible to determine the critical slipping rate by measuring the rotation rate of the particle at a single external rotation rate that is greater than the critical slipping rate, e.g. when $\Omega > \Omega_c$. Recall that the equation for the nonlinear rotational regime is

$$\left\langle \frac{d\theta}{dt} \right\rangle = \Omega - \sqrt{\Omega^2-\Omega_c^2}, \quad \Omega > \Omega_c. \tag{17}$$

By solving Eq. (17) for the critical slipping rate, we see that

$$\Omega_c = \langle\dot{\theta}\rangle^{1/2}[2\Omega-\langle\dot{\theta}\rangle]^{1/2} = \frac{mB}{\kappa\eta V}. \tag{18}$$

With Eq. (18), one can determine physical values by measuring one average nonlinear rotation rate, namely by solving for $m$, $B$, $\kappa$, $\eta$, or $V$. This makes measuring physical changes, such as viscosity or volume changes, especially straightforward and fast. This is the technique used to measure the viscosity changes in Section 4.3 as well as the binding and dissociation events in the experiments in Section 4.4.

### 2.6. Example of real-time measurements: viscosity

By using Eq. (18) a variety of parameters can be measured in near real-time, and here we give the theoretical example of viscosity. When monitoring a nonlinear rotating sphere in a fluid, the average rotation rate, $\langle\dot{\theta}\rangle$, will change when the viscosity is changed. One way to change the viscosity of a fluid is to alter its temperature. The temperature dependence of glycerol–water mixtures has been accurately characterized and is given by $\nu = \nu(T) = \exp(a+bT+cT^2)$ [37] and the critical slipping rate can therefore be rewritten as

$$\Omega_c(\nu(T)) = \frac{mB}{\rho\kappa V}\frac{1}{\exp(a+bT+cT^2)}, \tag{19}$$

where $a$, $b$, and $c$ are material-dependant constants [37]. If $\Omega_c$ is measured in a fluid with a known viscosity at $T_1$, the temperature is changed to $T_2$, and $\Omega_c$ is measured again, then the viscosity of the fluid at $T_2$ can be calculated, namely

$$\nu(T_2) = \frac{\nu(T_1)\Omega_c(T_1)}{\Omega_c(T_2)} = \nu(T_1)\left[\frac{\langle\dot{\theta}\rangle_{T_1}}{\langle\dot{\theta}\rangle_{T_2}}\right]^{1/2}\left[\frac{2\Omega-\langle\dot{\theta}\rangle_{T_1}}{2\Omega-\langle\dot{\theta}\rangle_{T_2}}\right]^{1/2} \tag{20}$$

This is the technique that is used in Section 4.3 to measure viscosity and is especially useful when the exact value of the particle volume or magnetic moment is unknown.

## 3. Experimental

### 3.1. Preparation of magnetic particles

#### 3.1.1. Preparation of fluorescent half-shell particles

Fluorescent magnetic microspheres with a diameter of 4.6 μm, obtained from Spherotech Inc. (Libertyville, IL), see Fig. 3(a), were dispersed into a monolayer supported by a glass substrate. This slide was then placed into a vacuum chamber where aluminum was vapor deposited at thicknesses well above the skin depth, e.g. 20–60 nm. The substrate was then placed in a magnetic field of ~1000 Oe. The particles were removed from the substrate via a small damp paintbrush. The paintbrush was sonicated in a small amount of water, typically 100–400 μL, where the particles could then be further diluted with glycerol for the experiments listed below. Sufficient dilution is necessary to inhibit aggregation on the time-scale of the experiment (see ref. [35]). The particles fabricated in this way were used in Sections 4.1–4.3. A major drawback to this method is that the commercial magnetic particles have a high degree of sphere-to-sphere nonuniformity in both size and content of magnetic material [42].

#### 3.1.2. Preparation of uniform half-shell particles

To improve uniformity over the commercial spheres described in Section 3.1.1, we fabricated uniform magnetic half-shell particles. The particles were fabricated using a method previously developed in our lab [10]. 1.86 μm silica microspheres (Bangs Labs Fishers, IN) were dispersed into a monolayer on a glass substrate by spreading the manufacturer's

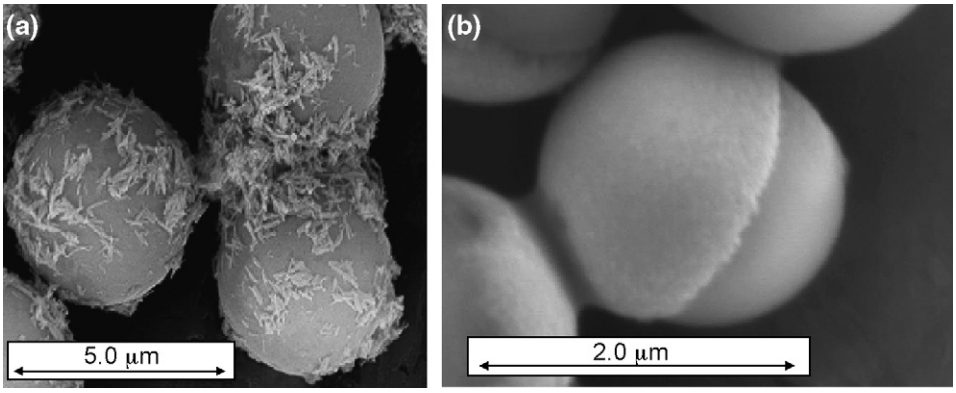


Fig. 3. Electron microscopy images of (a) fluorescent magnetic microspheres with a diameter of 4.6 μm (before aluminum was coated) and (b) 1.86 μm non-magnetic silica microspheres coated with 6, 90, and 6 nm layers of silver, iron and silver, respectively.

stock solution of spheres over an area of a ∼1.0 $cm^2$ and spin coating the slide. Varying layers and thicknesses of metal were then coated onto the spheres, in the following order: 6 nm of silver, 90 nm of iron, and 6 nm of silver. An example of the resulting spheres is shown in Fig. 3(b). Spheres were then removed and suspended as described in Section 3.1.1 and used for the experiments discussed in Sections 4.4 and 4.5.

### 3.2. Magnetic rotation

All particles were observed in homemade ∼100 μm thick fluidic cells. Rotation was carried out with a digital function generator used to rotate a stepper motor connected to a 1.6 cm diameter diametrically magnetized Alnico magnet (Dexter Magnetics Inc.). The magnet was placed in a horizontal orientation above the sample of interest at distances of 4–10 cm. This distance produced magnetic field values on the order of ∼5–20 Oe. The particle under study was observed to be actively rotated by this external rotation field, and since no translation was observed, any magnetic gradient forces produced by the external field were negligible. Also, with the setup used in our experiments, no significant gradient is expected over the microdomain of one particle.

### 3.3. Microscopy

All microscopic images used to measure half-shell intensity or reflection were obtained with a Roper Coolsnap ES CCD camera (Roper Scientific Tucson, AZ) connected to an inverted epifluorescence microscope (Olympus, Center Valley, PA) in various configurations. The microscope was either operated in fluorescence mode, with the appropriate fluorescence filter cube, or in reflection mode, with a 50% reflection/50% transmission cube. In both cases a Xenon lamp was used either for reflection or to excite fluorescence of the particles. To observe the particles, a 60× (NA = 0.85) objective lens was used in all experiments except binding detection and surface viscosity experiments, where a 100× (NA = 1.25) immersion lens was used. Shown in Fig. 4 is the microscopy setup used. Scanning electron microscopy images of the dried particles were obtained for characterization using a Phillips XL30 field emission gun.

### 3.4. Image acquisition and analysis

All images were acquired and analyzed using Metamorph software (Universal Imaging Corp., Sunnyvale, CA). Metamorph's ability to measure intensities of pixels of designated regions of interest was used to measure the time-dependant intensity or reflection from individual particles. A fluorescent particle will have one intensity peak per rotation but a particle monitored using reflection will have two intensity peaks per rotation. This dual peak behavior is a result of the light reflecting off both the convex and concave side of the metallic coating. The intensity expresses a sine-like dependence on the angle of the particle, thus making it possible to monitor the orientation of the particle. A fast Fourier transform was applied to the intensity time series to obtain an estimate of the average rotation at varying frequencies of the external rotation rate. Finally, a least squares fit was used to fit Eq. (8) to experimental results. This was the analysis method used in Sections 4.1 and 4.6.

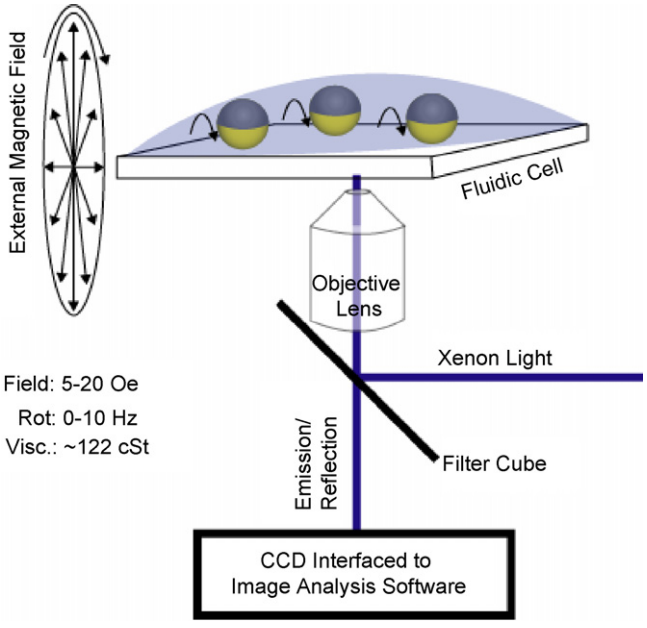


Fig. 4. Experimental microscopy setup used to monitor the rotation of half-shell particles.

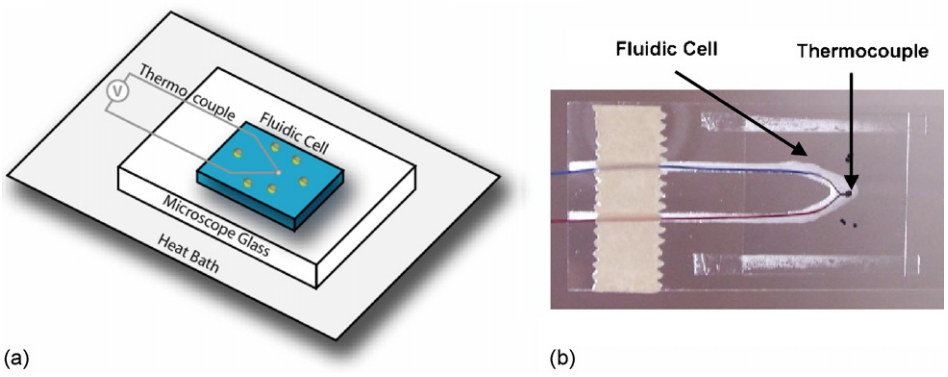


Fig. 5. Schematic representation of (a) the experimental setup used to obtain rotational images and to excite fluorescence and (b) a ~100 μm thick homemade fluidic cell interfaced with a T-type thermocouple (one lead is copper and the other is constantan).

Alternatively, with the measurement of a single average rotation rate at external driving frequencies $\Omega > \Omega_c$, the techniques described in Section 2.5 can be used to calculate the critical slipping rate. This was the analysis method used in Sections 4.2–4.5.

### 3.5. Temperature control and monitoring

The particles prepared in Section 3.1.1 were suspended in a 0.95 glycerol–water mass fraction. This solution was placed in a sealed homemade fluidic cell that contained a T-type thermocouple, as shown in Fig. 5. The error in temperature measurements were ±1 °C. All thermocouple readings were taken when the magnetic field was not rotating to eliminate the effects of currents induced in the leads by the changing field. The fluidic cell was heated with a heat bath that was in contact with the cell. In this experiment and analysis, kinematic viscosity was used rather than dynamic viscosity because it has been reported that many of the dynamic viscosity tables are not accurate [37]. In the same paper the authors accurately measured the kinematic viscosity of glycerol–water mixtures [37]. All other sections will report viscosity as dynamic as is the convention with phase-slipping experiments.

### 3.6. Particle binding experiments

In Section 4.4, we describe the association and dissociation of a Dynal MyOne 1.0 μm paramagnetic bead with a 1.86 μm half-shell particle (preparation discussed in Section 3.1.2). The association of the 1.0 and 1.86 μm half-shell particle was possible due to small magnetic interactions, while dissociation was performed using radiation pressure from a focused near-infrared Ti:Sapphire (Spectra Physics, Mountain View, CA) laser beam operating in continuous wave mode. Dissociation was induced by applying a 30 ms pulse of the focused light to the point of contact between the particles. The interference pattern of the beam reflected off the bottom glass surface of the fluidic cell, was also used to determine the approximate depth of the particles in the cell (where the particle was well over a diameter in distance from the glass-fluid interface). This allowed for reproducibility measurements as seen in Section 4.4. Optical filters were used to block the reflected near-infrared light from reaching the CCD camera.

## 4. Results and discussion

The linear-to-nonlinear rotation of magnetic particles rotated by an external driving field has a variety of promising applications. All applications presented here involve calculation of the critical slipping rate, determined either by fitting a series of measurements at different external rotation rates as outlined in Section 3.4 or by calculating the critical rate from a single nonlinear rotation measurement as outlined in Section 2.5. These two methods are similar except that the fitting method has reduced error because more measurements are made to determine $\Omega_c$.

### 4.1. Measurement of magnetic field

To demonstrate a nonlinear magnetic micro-oscillator's rotational dependence on external magnetic field strength, the magnitude of the magnetic field was changed and the critical slipping rate was measured. This was accomplished by increasing the distance between a rotating magnet and the sample plane. Solving for $B$ in Eq. (16) yields

$$B = \frac{\kappa \eta V \Omega_c}{m} \tag{21}$$

Thus, the magnetic field is proportional to the critical slipping rate ($B \propto \Omega_c$). While it is possible to use this technique to determine $B$, it is most likely an impractical endeavor. It is impractical not in its ability to determine $B$, but in that there are few situations where the magnetic field of interest is applicable; the magnetic field must be rotating at a constant angular rate and be immersed in a fluid. It is in these situations – where local rotational fields or rotational fields on small dimensions are of interest – that application of critical phase-slipping for measurement of magnetic fields shows the most promise. The ability to measure a change in magnetic field strength using our nonlinear oscillators is demonstrated by Fig. 6. The external magnetic field strength was changed from 87 to 30 Oe, and accordingly the critical slipping rate changed from 5.81 to 2.15 rad/s. This change is to within ~7.3% of that expected from Eq. (21). While in this experiment the critical slipping rate was determined by means of a least squares fit, it is also possible to perform near real-time measurements on a changing magnetic field, by measuring the

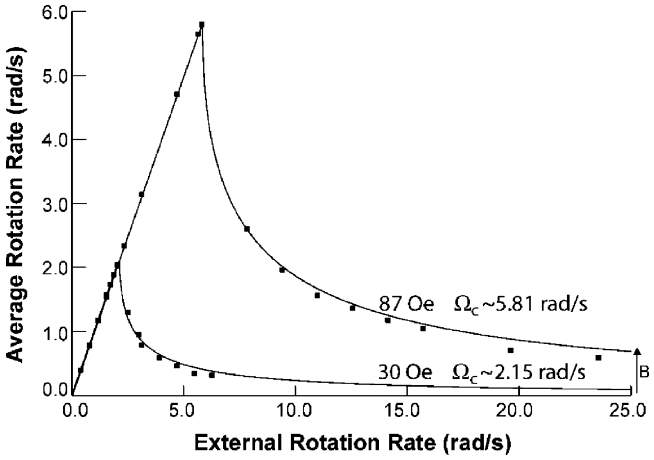


Fig. 6. Rotational dynamics of a 4.6 μm particle for two different magnetic fields. The magnetic field value was changed from 87 to 30 Oe and the critical slipping rate changed from 5.81 to 2.15 rad/s.

average rotation rate, namely

$$B_2 = \frac{B_1\Omega_c(B_2)}{\Omega_c(B_1)} = B_1\left[\frac{\langle\dot{\theta}\rangle_{B_2}}{\langle\dot{\theta}\rangle_{B_2}}\right]^{1/2}\left[\frac{2\Omega - \langle\dot{\theta}\rangle_{B_2}}{2\Omega - \langle\dot{\theta}\rangle_{B_2}}\right]^{1/2}. \quad (22)$$

### 4.2. Measurement of inter-particle magnetic moment uniformity

In general, magnetic microspheres have found many uses in biomedical applications, and in these applications the microspheres' magnetic characteristics are crucial [43]. In particular, the type of magnetism, i.e. paramgnetism, superparamagnetism, or ferromagnetism, that the particles exhibit [43] and their uniformity of magnetic responsiveness [42] are important. The magnetic moment of microspheres that rotate in response to an externally rotating magnetic field can be determined by measuring the critical slipping rate. As with magnetic fields, the magnetic moment is proportional to the critical slipping rate, namely

$$m = \frac{\kappa\eta V\Omega_c}{B} \quad (23)$$

Ultimately, this enables the measurement of the magnetic moment of single magnetic nanoparticles and microspheres. If the parameters in Eq. (23) such as $B$, $\kappa$, $V$, or $\eta$ cannot be determined, then the variation in the critical slipping rate will provide an estimation of the variation of the magnetic responsiveness rather than determining a value for $m$.

Several techniques have emerged to measure single particle and ensemble magnetic moments and magnetic responsiveness. Häfeli et al. [42], using a technique other than described here, have shown that commercially available magnetic particles vary in their magnetophoretic response from 30% to 80%. We have performed uniformity measurements for the particles described in Sections 3.1.1 and 3.1.2. The half-shell reflection particles made by vapor deposition, described in Section 3.1.2, had a variation in their magnetic responsiveness, i.e. standard deviation, of ~16%. Commercially obtained particles had a variation in magnetic responsiveness of ~50%, which is consistent with Häfeli's results. These values were measured through the nonlinear rotation of the half-shell particles. Generally, the magnetic moments of micro and nanoparticles are determined from ensemble measurements, where an average value for the magnetic moment is determined for the ensemble. Korneva et al. [17] even used critical slipping to estimate the moment of magnetically loaded carbon nanotubes, but also monitored many particles at once, i.e. an ensemble value. In contrast, determining the critical slipping rate for individual particles, allows one to determine single particle magnetic moments and magnetic uniformity of an ensemble of particles.

### 4.3. Measurement of viscosity

In a viscous fluid, measurement of $\Omega_c$ allows for the measurement of properties like the dynamic viscosity:

$$\eta = \frac{mB}{\kappa V\Omega_c}. \quad (24)$$

If all of the microparticles have the same shape, volume, and magnetic content, it would be possible to measure a spatial distribution of viscosity. This ability could be applied to complex fluids where pores of various sizes and spacings are present. By using these spatially resolved viscometers, the effective viscosity at various points in the complex fluid could be measured. Thus, this technique may be a useful addition to the growing list of colloidal probes used for microrheology [44].

Unfortunately, current commercial magnetic particles do not have high enough particle-to-particle uniformity in size or magnetic content to enable accurate spatial viscosity measurements using the technique described here. Using a single probe, however, it is possible to perform viscosity experiments. For example, the viscosity of glycerol has an exponential dependence on temperature, see Eq. (19). The critical slipping rate for a single magnetic particle can be monitored while the temperature in a glycerol solution is altered. From Eq. (20), it is clear that the critical slipping rate and, therefore, the nonlinear rotation rate of a rotationally driven microprobe can be used to determine viscosity as long as the starting viscosity is known.

We have demonstrated such an application by rotating particles in a 0.95 glycerol mass fraction solution and increasing the temperature of the glycerol–water mixture. The nonlinear rotation rate changes with temperature, increasing as temperature is increased, as shown in Fig. 7(a). With this type of measurement one can calibrate the nonlinear rotation rate versus viscosity as shown in Fig. 7(b). By combining this technique with optical tweezers, it may be possible to manipulate the magnetic particle [20,28], after viscosity calibration, in more interesting systems like biological environments or near fluid-solid or fluid-air interfaces. From the work of Shankar and Kumar [37] it was possible to compare our experimental $\nu(T)$ with their reported $\nu(T)$. Table 1 shows this comparison, where the various viscosities were calculated using Eq. (20). The values of $a$, $b$, and $c$ used to fit the data in Fig. 7 for a 0.95 glycerol-water mass fraction were slightly different from that of ref. [37], but all calculated

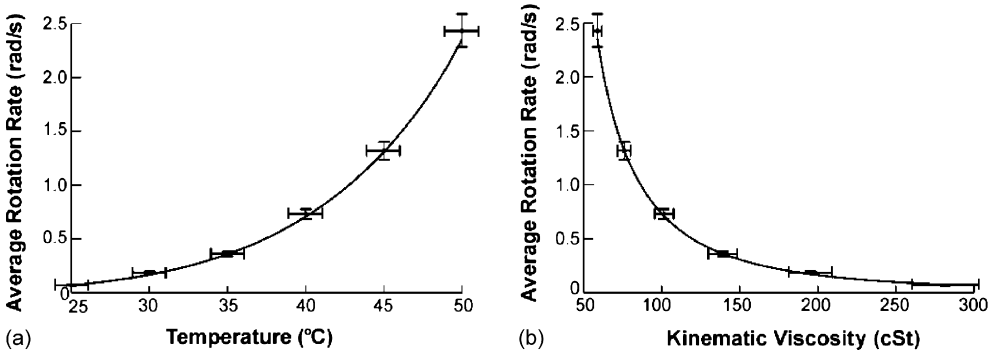


Fig. 7. Experimentally obtained values for the average rotation rate, where the line is a theoretical fit using Eqs. (18) and (19), where $a = 5.23$, $b = -0.16$, and $c = .0013$, plotted vs. (a) temperature and (b) the temperature dependent kinematic viscosities. Error bars in the average rotation rate correspond to an average error of ∼6.5% obtained from measuring several average rotation rates over a variety of external rotation rates and error bars in the value axis for (a) are from a 1 °C error in thermocouple measurements and (b) the resulting errors in calculated viscosity from the 1 °C error.

viscosity values had less than an 8% discrepancy from their reported values.

### 4.4. Measurement of binding dynamics

Particle size is a significant variable in the critical slipping equation. This significance is more apparent when considering a sphere. Substituting the volume of a sphere and a sphere's shape factor of 6 into Eq. (16), we obtain

$$\Omega_c = \frac{mB}{8\pi r_h^3}, \tag{25}$$

where $r_h$ is the hydrodynamic radius. Eq. (25) indicates that $\Omega_c$ strongly depends on the radius of the rotating particle system. The effective shape and volume of the system can be changed by attachment to other objects such as other magnetic particles or biological agents like bacteria, viruses or proteins.

The ability to detect biological particles has become a highly pursued field of study and much attention has been directed toward nanoelectromechanical (NEMs) and other microscale oscillators [45,46]. These oscillators are cantilevers that have a natural oscillation frequency that changes when a biological agent binds to their functionalized surface. In this way, single bioparticles have been detected [47,48]. While NEMs are very effective at detecting biological agents in vacuum or in air, they have not been applied to continuous monitoring in fluids. In air or in vacuum environments cantilever-based systems are extremely sensitive to physical changes [49]; however, due to viscous losses, this sensitivity decreases drastically when cantilevers are operated in fluids [50–52]. For this reason, the need to develop a small scale oscillating system that is capable of continuous monitoring in fluid environments remains. One potential system that addresses this need is the magnetic nonlinear microoscillator.

Table 1
Measured values of $\Omega_c$, at increasing temperatures, used to calculate kinematic viscosities

| Temperature (°C) | $\Omega_c$ | $\Omega_c$ ratios | Calculated, $\nu$ (cSt) | Reported, $\nu$ (cSt) [37] |
|---|---|---|---|---|
| 25 | 0.128 | NA | NA | 283 |
| 30 | 0.207 | 0.620 | 175.4 | 194 |
| 35 | 0.286 | 0.447 | 126.6 | 137 |
| 40 | 0.400 | 0.320 | 90.5 | 95.4 |
| 45 | 0.519 | 0.246 | 69.7 | 69.8 |
| 50 | 0.656 | 0.195 | 55.2 | 54.2 |

Calculated viscosities were performed with Eq. (20) and an assumed viscosity of 283 cSt at 25 °C. The rightmost column is reported viscosities from Ref. [37].

Due to the deterministic behavior of a nonlinear rotating magnetic particle (see Eq. (18)), $\Omega_c$ can be calculated with the measurement of only one nonlinear rotation rate. Determining $\Omega_c$ in this way, however, is susceptible to more error than in the case of measuring several values of $\langle\dot{\theta}\rangle$ followed by least-squares fitting the data points. For example, $\Omega_c$ was calculated with single average rotation rates at external rates of $\Omega > \Omega_c$ and the average difference between the value of $\Omega_c$ determined from a least-squares fit (as described in Section 3.4) and that determined from one value of $\langle\dot{\theta}\rangle$ was found to be only ∼1.4%. Such low errors allow for accurate measurement of $\Omega_c$ which translates to more accurate measurement of the changes in drag of a single particle before and after a binding event. In the case of a paramagnetic particle binding to a half-shell particle, used to simulate a biological agent, see Fig. 8(a), where changes in $m$ of the system are negligible,

$$\frac{\Omega_{c1}}{\Omega_{c2}} = \frac{mB/\eta\kappa_1 V_1}{mB/\eta\kappa_2 V_2} = \frac{\kappa_2 V_2}{\kappa_1 V_1} \tag{26}$$

$$\Rightarrow \frac{\kappa_2 V_2}{\kappa_1 V_1} = \left[\frac{\langle\dot{\theta}_1\rangle}{\langle\dot{\theta}_2\rangle}\right]^{1/2}\left[\frac{2\Omega - \langle\dot{\theta}_1\rangle}{2\Omega - \langle\dot{\theta}_2\rangle}\right]^{1/2} \tag{27}$$

The first term on the right hand side of Eq. (27) is the dominating factor, especially for large external rotation rates ($\Omega \gg \langle\dot{\theta}_1\rangle > \langle\dot{\theta}_2\rangle$). The second term acts as a correction factor that approaches unity as $1 + O(\langle\dot{\theta}_1\rangle/\Omega, \langle\dot{\theta}_2\rangle/\Omega)$.

Using the procedure described above, the changes in the volume and shape were monitored, when a 1.0 μm paramagnetic particle was bound to a 1.89 μm magnetic half-shell particle, by measuring the change in the average nonlinear rotation rate. Fig. 8(b) indicates this change, where the average rotation rate shifts from ∼0.44 rot/s before binding to ∼0.1 rot/s after binding, with a measurement error of ∼2%. These measurements were reproducible and are shown in Fig. 8(c).

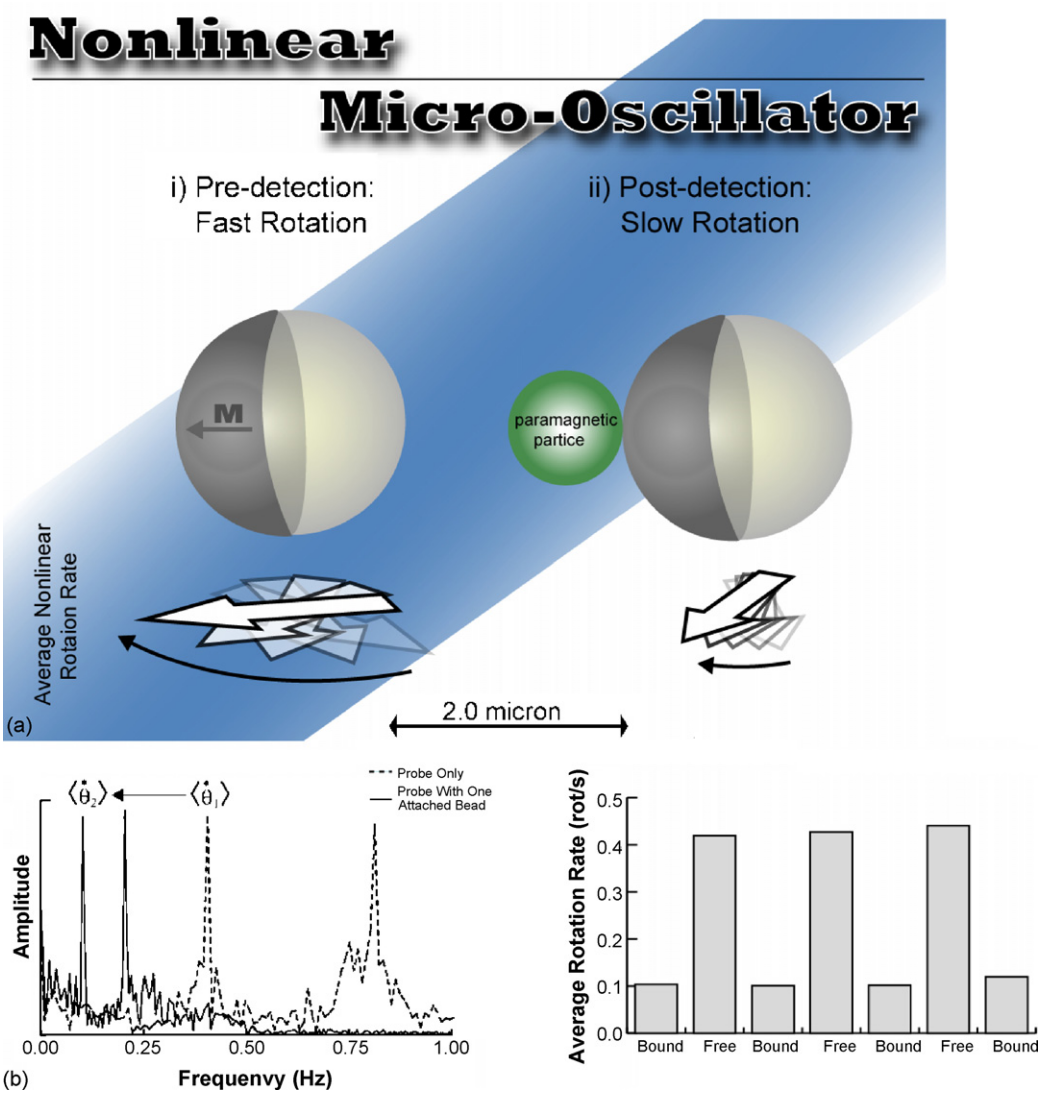


Fig. 8. (a) Schematic representation of the average nonlinear rotation rates of a micro-oscillator before and after the detection of an antigen mimicked by a 1.0 μm paramagnetic sphere. (b) Rotation rate shown before and after rotation, where the second peak in each spectrum is from the micro-oscillator reflecting twice per rotation. (c) Average nonlinear rotation rates for sequential single particle attachment and detachment events.

Between measurements the system was either manipulated with a Ti:Sapphire laser beam (see Section 3.6) to dissociate the particles, or left undisturbed to allow the particles to reattach. Eq. (27) also allows for the approximation of the volume of the paramagnetic particle. From the rotational values ∼0.44 and ∼0.1 rot/s, the approximated diameter of the bound sphere was found to be ∼1.08 μm and the estimated diameter from scanning electron microscopy was 1.01 μm [53]. Thus, the capability of using this system to measure drag changes caused by a foreign object attaching to the micro-oscillator's surface has been demonstrated. An identical procedure as to that outlined here could be used to detect a biological agent, such as a single bacterium. Finally, we suggest that if a bacterium is attached to a magnetic particle and then grows, the effective hydrodynamic radius and shape factor of the system will be changed. Our early experiments suggest that errors in the critical slipping rate are on the order of ∼2%. With this percentage, use of a 500 nm magnetic particle (currently under fabrication), which we are currently fabricating, could facilitate detection of single 100 nm biological agents. This size range encompasses such viruses that affect human cells like HIV, smallpox, influenza, and Ebola. Larger bacteria such as tuberculosis and Escherichia coli are already within the sensing capability of the above 1.89 μm half-shell particles. Preliminary experiments with Escherichia coli have resulted in easy and reproducible detection of single bacteria, where the nonlinear rotation rate was reduced by a factor of ∼3.8 when bacteria were attached.

### 4.5. Estimation of shape factor

It is possible to use the nonlinear rotation of magnetic particles to measure the shape factor, $\kappa$. To calculate the effect of a shape factor change, one needs only to double the magnetic moment and the volume of the micro-system. These two changes will have a canceling effect. If the original particles shape is known, then $\kappa_1$ will be well defined, e.g. for a sphere

it would be 6. With this value, and measurement of the two critical slipping rates, $\kappa_2$ can be found from the relationship

$$\kappa_2 = \kappa_1 \frac{\Omega_c(\kappa_1)}{\Omega_c(\kappa_2)} \tag{28}$$

We performed this measurement for two 1.86 μm half-shell particles binding to each other and found the value for $\kappa_2$ for the two-sphere system to be ∼17 [53]. This value is between the shape factor for a sphere, which is 6, and that of a system of three spheres, which is 44 [16].

### 4.6. Physiochemical sensor

Combining the techniques and methods thus far described with chemical sensing probes could yield a powerful physiochemical sensor [9]. We have previously suggested and demonstrated such a probe [8]. By measuring the nonlinear rotation of a magnetic particle, one can measure all of the physical properties discussed in this manuscript. Then, through the use of a fluorescent indicator dye located within the particle, or some equivalent synergistic scheme, local chemical concentrations can be measured [8]. Such a probe would be useful in elucidating the interplay between physical and chemical properties in live biological embryos or cells. It is also possible to add the physical probing capabilities to chemical sensors in a one step fabrication process, namely vapor deposition of magnetic materials [10].

## 5. Conclusions

The nonlinear rotation of driven magnetic microparticles offers a new tool to investigate a variety of physical properties on a very small scale and has the potential to be combined with chemical sensing. Here, we have demonstrated many of the physical applications, including viscosity measurements, magnetic field measurements, measurement of magnetic particle characteristics, measurements of binding events through changes in volume, and physiochemical sensors. The optimization of this new arena of applications will allow for the realization of a new generation of micro- and nano-tools.

## Acknowledgements

The authors would like to thank Roy Clarke and Vladimir Stoica for help with the fabrication of the reflection half-shell particles, Keith Bonin from Wake Forest University for helpful theoretical discussions, Jeffrey N. Anker for theory discussion and experimental setup, and Karen A. Kehbein for assistance with the physiochemical sensors. We also would like to acknowledge DARPA Bio-Magnetics grant F008406 and NSF grant DMR 9900434 for financial support. SEM images were acquired at the EMAL facility at the University of Michigan.

## References

[1] Q.A. Pankhurst, J. Connolly, S.K. Jones, J. Dobson, Applications of magnetic nanoparticles in biomedicine, J. Phys. D: Appl. Phys. 36 (2003) R167–R181.
[2] M.A.M. Gijs, Magnetic bead handling on-chip: new opportunities for analytical applications, Microfluidics Nanofluidics 1 (2004) 22–40.
[3] R.S. Molday, S.P.S. Yen, A. Rembaum, Application of magnetic microspheres in labelling and separation of cells, Nature 268 (1977) 437–438.
[4] B.I. Haukanes, C. Kvam, Application of magnetic beads in bioassays, Bio-Technology 11 (1993) 60–63.
[5] M. Albrecht, G. Hu, I.L. Guhr, T.C. Ulbrich, J. Boneberg, P. Leiderer, G. Schatz, Magnetic multilayers on nanospheres, Nat. Mater. 4 (2005) 203.
[6] C.J. Behrend, J.N. Anker, B.H. McNaughton, R. Kopelman, Microrheology with modulated optical nanoprobes (MOONs), J. Magn. Magn. Mater. 293 (2005) 663–670.
[7] A. Cēbers, M. Ozols, Dynamics of an active magnetic particle in a rotating magnetic field, Phys. Rev. E 73 (2006) 021505.
[8] B.H. McNaughton, K.A. Kehbein, J.N. Anker, R. Kopelman, Sudden breakdown in linear response of a rotationally driven magnetic microparticle and application to physical and chemical microsensing, J. Phys. Chem. B 110 (2006) 18958–18964.
[9] G. Bao, S. Suresh, Cell and molecular mechanics of biological materials, Nat. Mater. 2 (2003) 715–725.
[10] B.H. McNaughton, V. Stoica, J.N. Anker, R. Clarke, R. Kopelman, Fabrication of uniform half-shell mangetic nanoparticles and microspheres with applications as magnetically modulated optical nanoprobes, http://arxiv:cond-mat/0506418 (2005).
[11] M. Brasuel, R. Kopelman, T.J. Miller, R. Tjalkens, M.A. Philbert, Fluorescent nanosensors for intracellular chemical analysis: decyl methacrylate liquid polymer matrix and ion exchange-based potassium PEBBLE sensors with real-time application to viable rat C6 glioma cells, Anal. Chem. 73 (2001) 2221–2228.
[12] H.A. Clark, R. Kopelman, R. Tjalkens, M.A. Philbert, Optical nanosensors for chemical analysis inside single living cells. 2. Sensors for pH and calcium and the intracellular application of PEBBLE sensors, Anal. Chem. 71 (1999) 4837–4843.
[13] H.A. Clark, M. Hoyer, M.A. Philbert, R. Kopelman, Optical nanosensors for chemical analysis inside single living cells. 1. Fabricaiton, characterization, and methods for intracellular delivery of PEBBLE sensors, Anal. Chem. 71 (1999) 4831–4836.
[14] E. Monson, M. Brasuel, M.A. Philbert, R. Kopelman, PEBBLE nanosensors for in vitro bioanalysis, in: T. Vo-Dinh (Ed.), Biomedical Photonics Handbook, CRC Press, 2003.
[15] H. Xu, J.W. Aylott, R. Kopelman, T.J. Miller, M.A. Philbert, A real-time ratiometric method for the determination of molecular oxygen inside living cells using sol-gel-based spherical optical nanosensors with applications to rat C6 glioma, Anal. Chem. 73 (2001) 4124–4133.
[16] S.L. Biswal, A.P. Gast, Micromixing with linked chains of paramagnetic particles, Anal. Chem. 76 (2004) 6448–6455.
[17] G. Korneva, H. Ye, Y. Gogotsi, D. Halverson, G. Friedman, J.C. Bradley, K.G. Kornev, Carbon nanotubes loaded with magnetic particles, Nano Lett. 5 (2005) 879–884.
[18] A.W. Shelton, K.D. Bonin, T.G. Walker, Nonlinear motion of optically torqued nanorods, Phys. Rev. E 71 (2005) 036204.
[19] J.N. Anker, C.J. Behrend, R. Kopelman, Aspherical magnetically modulated optical nanoprobes MagMOONs, J. Appl. Phys. 93 (2003) 6698.
[20] R.R. Agayan, T. Horvath, B.H. McNaughton, J.N. Anker, R. Kopelman, Optical manipulation of metal-silica hybrid nanoparticles, Proc. SPIE 5514 (2004) 502–513.
[21] J.N. Anker, T. Horvath, R. Kopelman, Cooking with nanoparticles: a simple method of forming roll, pancake, and breaded polystyrene microparticles, Eur. Cells Mater. 3 (2002) 34.
[22] J.N. Anker, R. Kopelman, Magnetically modulated optical nanoprobes, Appl. Phys. Lett. 82 (2003) 1102.
[23] J.N. Anker, C.J. Behrend, B.H. McNaughton, T.G. Roberts, M. Brasuel, M.A. Philbert, R. Kopelman, Characterization and applications of modulated optical nanoprobes (MOONs), Mater. Res. Soc. Symp. Proc. (2004).
[24] J.N. Anker, C.J. Behrend, R. Kopelman, Magnetically modulated optical nanoprobes (MagMOONs) and systems, J. Magn. Magn. Mater. 293 (2005) 655–662.
[25] C.J. Behrend, J.N. Anker, B.H. McNaughton, M. Brasuel, M.A. Philbert, R. Kopelman, Metal-capped brownain and magnetically modulated opti-

cal nanoprobes (MOONs): micromechanics in chemical and biological microenvironments, J. Phys. Chem. B 108 (2004) 10408.
[26] B.H. McNaughton, J.N. Anker, R. Kopelman, Magnetic microdrill as a modulated fluorescent pH sensor, J. Magn. Magn. Mater. 293 (2005) 696–701.
[27] Y. Lu, G.L. Liu, J. Kim, Y.X. Mejia, L.P. Lee, Nanophotonic crescent moon structures with sharp edge for ultrasensitive biomolecular detection by local electromagnetic field enhancement effect, Nano Lett. 5 (2005) 119.
[28] F.S. Merkt, A. Erbe, P. Leiderer, Capped colloids as light-mills in optical traps, http://arxiv:cond-mat/0605463 (2006).
[29] V.N. Paunov, O.J. Cayre, Supraparticles, Janus particles fabricated by replication of particle monolayers at liquid surfaces using a gel trapping technique, Adv. Mater. 16 (2004) 788.
[30] K.H. Roh, D.C. Martin, J. Lahann, Biphasic Janus particles with nanoscale anisotropy, Nat. Mater. 4 (2005) 759–763.
[31] A. Perro, S. Reculusa, S. Ravaine, E. Bourgeat-Lami, E. Duguet, Design and synthesis of Janus micro-and nanoparticles, J. Mater. Chem. 15 (2005) 3745–3760.
[32] J.C. Love, B.D. Gates, D.B. Wolfe, K.E. Paul, G.M. Whitesides, Fabrication and wetting properties of metallic half-shells with submicron diameters, Nano Lett. 2 (2002) 891–894.
[33] Y. Lu, H. Xiong, X. Jiang, Y. Xia, M. Prentiss, G.M. Whitesides, Asymmetric dimers can be formed by dewetting half-shells of gold deposited on the surfaces of spherical oxide colloids, J. Am. Chem. Soc. 125 (2003) 12724–12725.
[34] J.J. Newman, R.B. Yarbrough, Motions of a magnetic particle in a viscous medium, J. Appl. Phys. 39 (1968) 5566.
[35] P.A. Valberg, J.P. Butler, Magnetic particle motions within living cells, Biophys. J. 52 (1987) 537–550.
[36] M. Gitterman, Order and chaos: are they contradictory or complementary, Eur. J. Phys. 23 (2002) 119–122.
[37] P.N. Shankar, M. Kumar, Experimental determination of the kinematic viscosity of glycerol–water mixtures, Proc. R. Soc. Lond. A 444 (1994) 573–581.
[38] E.M. Purcell, Life at low Reynolds number, Am. J. Phys. 45 (1977) 3–11.
[39] S.H. Strogatz, Nonlinear Dynamics and Chaos, Westview Press, Cambridge, MA, 2000, # of pages.
[40] A. Yamazaki, M. Sendoh, K. Ishiyama, T. Hayase, K.I. Arai, Three-dimensional analysis of swimming properties of a spiral-type magnetic micro-machine, Sens. Actuators A 105 (2003) 103–108.
[41] K. Ishiyama, M. Sendoh, A. Yamazaki, M. Inoue, K.I. Arai, Swimming of magnetic micro-machines under a very wide-range of Reynolds number conditions, IEEE Trans. Magn. 37 (2001).
[42] U.O. Häfeli, R. Ciocan, J.P. Dailey, Characterization of magnetic carriers and their magnetophoretic mobility using a digital microscopy method, Eur. Cells Mater. 3 (2002) 24–27.
[43] J. Connolly, T.G. St. Pierre, J. Dobson, Experimental evaluation of the magnetic properties of commercially available magnetic microspheres, Bio-Med. Mater. Eng. 15 (2005) 421–431.
[44] T.A. Waigh, Microrheology of complex fluids, Rep. Prog. Phys. 68 (2005) 685–742.
[45] K.L. Ekinci, M.L. Roukes, Nanoelectromechanical systems, Rev. Sci. Instrum. 76 (2005) 061101.
[46] A.M. Fennimore, T.D. Yuzvinsky, W.Q. Han, M.S. Fuhrer, J. Cumings, A. Zettl, Rotational actuators based on carbon nanotubes, Nature 424 (2003) 408.
[47] B. Ilic, D. Czaplewski, M. Zalalutdinov, H.G. Craighead, P. Neuzil, C. Campagnolo, C. Batt, Single cell detection with micromechanical oscillators, J. Vacuum Sci. Technol. B: Microelectron. Nanometer Struct. 19 (2001) 2825.
[48] B. Ilic, Y. Yang, H.G. Craighead, Virus detection using nanoelectromechanical devices, Appl. Phys. Lett. 85 (2004) 2604.
[49] S.S. Verbridge, J.M. Parpia, R.B. Reichenbach, L.M. Bellan, H.G. Craighead, High quality factor resonance at room temperature with nanostrings under high tensile stress, J. Appl. Phys. 99 (2006) 124304.
[50] R.B. Wang, Z.J. Bhiladvala, Effect of fluids on the Q factor and resonance frequency of oscillating micrometer and nanometer scale beams, Phys. Rev. E 69 (2004) 36307.
[51] M.R. Paul, M.C. Cross, Stochastic dynamics of nanoscale oscillators immersed in a viscous fluid, Phys. Rev. Lett. 92 (2004) 235501.
[52] J.F. Vignola, J.A. Judge, J. Jarzynski, M. Zalalutdinov, B.H. Houston, J.W. Baldwin, Effect of viscous loss on mechanical resonators designed for mass detection, Appl. Phys. Lett. 88 (2006) 041921.
[53] B.H. McNaughton, R.R. Agayan, R. Kopelman, submitted for publication.
[54] G. Helgesen, P. Pieranski, A.T. Skjeltorp, Nonlinear phenomena in systems of magnetic holes, Phys. Rev. Lett. 64 (1990) 1425–1428.

## Biographies

**Brandon H. McNaughton** (http://www.umich.edu/~bmcnaugh) obtained his BS in Physics from California State University, Bakersfield in 2002. Currently, he is researching and developing magnetic micro- and nanoparticle fabrication techniques and using magnetic particles for various sensing applications. This work is carried out as a PhD candidate in the Applied Physics Program at the University of Michigan under the direction of Professor Raoul Kopelman. He also founded and operates a nanotechnology based website, http://www.everydaynano.com/.

**Rodney R. Agayan** received his BS in Applied & Engineering Physics in 1997 from Cornell University. He worked as a research scientist on interference lithography at the Lawrence Livermore National Laboratory in Livermore, CA. He then received his MS in Applied Physics and in Electrical Engineering at the University of Michigan, 2003 and 2005. He is currently a PhD candidate in Applied Physics at the University of Michigan where his interests include laser tweezers and micro- and nanoparticle biosensors.

**Jane X. Wang** obtained her BS in Physics and a minor in math from the University of Oklahoma. She is currently pursuing her doctorate in Applied Physics at the University of Michigan, working on modeling complex systems and neural networks. She was awarded an honorable mention for the 2006 National Science Foundation Graduate Fellowship.

**Raoul Kopelman** (http://www.umich.edu/~koplab) is the Richard Smalley Distinguished University Professor of Chemistry, Physics, and Applied Physics at The University of Michigan, Ann Arbor, as well as a member of the Biophysics Program, Biomedical Engineering and the Center for Biological Nanotechnology, The Medical School. He obtained BS and Dipl Eng Degrees in Chemical Engineering from the Technion, Israel Institute of Technology, as well as an MS in Physical Chemistry. After having received a PhD in Chemistry from Columbia University, he spent 2 years as research associate at Harvard University, 2 years as an instructor at the Technion, and 2 years as senior research fellow at the California Institute of Technology before coming to Michigan. He is a fellow of the American Physical Society and the American Association for the Advancement of Science, and has received, among others, the American Chemical Society's Edward Morley Award and Medal (1997), as well as it is Spectrochemical Analysis Award (2005). Current research interests are in non-classical chemical reaction kinetics and in ultra-small optochemical sensors and actuators for biomedical use. Smart nanoprobes are being developed for the detection and therapy of cancer. Kopelman invented optical nanosensors for single cell chemical and physical imaging and is the co-inventor of targeted multifunctional nanoplatforms (TNP) for the imaging and therapy of tumors, as well as of a nanoscale photon source, a nanoscale voltmeter and a nanoscale viscometer.